Lithium-mediated Ammonia Synthesis from Water and Nitrogen: A Membrane-free Approach Enabled by Immiscible Aqueous/Organic Hybrid Electrolyte System

Journal:	*Green Chemistry*
Manuscript ID	GC-ART-04-2019-001338.R1
Article Type:	Paper
Date Submitted by the Author:	03-Jun-2019
Complete List of Authors:	Kim, Kwiyong; University of Illinois at Urbana-Champaign Chen, Yifu; Iowa State University Han, Jong-In; KAIST, Yoon, Hyung-Chul; Korea Institute of Energy Research, Li, Wenzhen; Iowa State University, Chemical & Biological Engineering Department

Green Chemistry

Article

Lithium-mediated Ammonia Synthesis from Water and Nitrogen: A Membrane-free Approach Enabled by Immiscible Aqueous/Organic Hybrid Electrolyte System

Received 00th January 20xx,
Accepted 00th January 20xx

DOI: 10.1039/x0xx00000x

www.rsc.org/

Kwiyong Kim,[†#a] Yifu Chen,[†a] Jong-In Han,[b] Hyung Chul Yoon[c] and Wenzhen Li*[ad]

Lithium-mediated pathway provides a promising way for facile and selective dissociation of nitrogen for ammonia synthesis. However, the prevailing electro-deposition of lithium, especially when coupled to the anodic oxygen evolution from water or hydroxide, presents disadvantages including the use of expensive Li-ion conducting ceramics (LISICON) or high temperature operation of molten salts. In this study, a membrane-free approach based on the immiscibility of aqueous/organic electrolytes was adopted for lithium electro-deposition, which could be utilized for subsequent nitridation and ammonia synthesis. We found that a biphasic system of aqueous 1 M $LiClO_4$ and 1 M $LiClO_4$/propylene carbonate reinforced with PMMA (poly(methyl methacrylate)) acts the same as a LISICON-based aqueous/organic hybrid electrolyte system, but without any physical membrane. With a fairly high faradaic efficiency (FE) of 57.2 % and production rate of 1.21×10^{-9} mol cm^{-2} s^{-1} for ammonia synthesis, this membrane-free approach and its application to ammonia synthesis provide an innovative way to the advancements in next-generation energy storage technologies.

Introduction

The Haber-Bosch process is a well-established ammonia (NH_3) synthesis technology which converts more than 170 million tons of nitrogen (N_2) to NH_3 every year.[1] This mature process, however, is exceedingly energy-intensive due to its harsh operational conditions, and suffers from extensive carbon emissions.[2-6] In light of these shortcomings, development of a more environmentally benign alternative is of absolute necessity.

Electrochemical synthesis is an attractive candidate because the energy consumption, if optimized, could be lowered compared to the Haber-Bosch process while avoiding immediate carbon emissions.[7-9] If the required electrical energy for the electro-synthesis is supplied from renewable sources, this approach will offer a way of energy storage into NH_3 as a next-generation, long-time energy carrier with an energy density higher than hydrogen, even close to that of fossil fuels.[10] Provided that water serves as an electron donor for this N_2-reducing reaction, NH_3 synthesis can be possible with nature's abundant and eco-friendly resources, thereby achieving a truly sustainable and decentralized process. In the last three decades, such electrochemical processes have been widely developed.[11-17] However, the faradaic efficiencies (FEs) were intolerably low in most cases because a significant fraction of the faradaic current becomes diverted toward an electron-stealing side reaction (e.g. hydrogen evolution), while the intended N_2 reduction is sluggish due to its inertness from the strong triple bond.[18-23] The judicious choice of materials and an electrochemical configuration is therefore undoubtedly required to overcome such obstacles and eventually achieve excellent selectivity toward the N_2 reduction.

Lithium (Li)-mediated reduction offers an innovative way of N_2 fixation. Li metal, on account of the negative potential of Li^+/Li (-3.04 V vs. SHE), spontaneously dissociates N_2 to form lithium nitride (Li_3N), a high energy precursor which is readily converted into NH_3 upon reaction with protons or water.[24-27] This Li-mediated approach, realized by a stepwise combination of Li deposition, nitridation, and NH_3 formation, gives advantageous features in that: (1) in a material selection perspective, highly reactive surface Li, with small barriers of N_2 activation, is an excellent N_2-reducing agent[24]; and (2) in an electrochemical

[a] Department of Chemical and Biological Engineering
Iowa State University
Ames 50011 (United States)
E-mail: wzli@iastate.edu
[b] Department of Civil and Environmental Engineering
Korea Advanced Institute of Science of Technology
Daejeon 34141 (Republic of Korea)
[c] Clean Fuel Laboratory
Korea Institute of Energy Research
Daejeon 34129 (Republic of Korea)
[d] US Department of Energy Ames Laboratory
Ames 50011 (United States)
[†] Kwiyong Kim and Yifu Chen contributed equally.
#Present address: Department of Chemical and Biomolecular Engineering
University of Illinois at Urbana-Champaign
Urbana, Illinois 61801 (United States)
Electronic Supplementary Information (ESI) available: [details of any supplementary information available should be included here]. See DOI: 10.1039/x0xx00000x

process perspective, its configuration allows to separate protic compounds (H_2O, H^+ and OH^-) from highly reactive cathodic surface Li by means of Li-ion conducting glass ceramics (LISICON) [25,27] or porous alumina diffusion barriers[24], thereby circumventing self-discharge of Li and hydrogen evolution. Unfortunately, however, developing economic Li deposition processes is still challenging due either to high temperature (molten salts approach), or to costly LISICON and its questionable chemical stability upon long-term operation.[28]

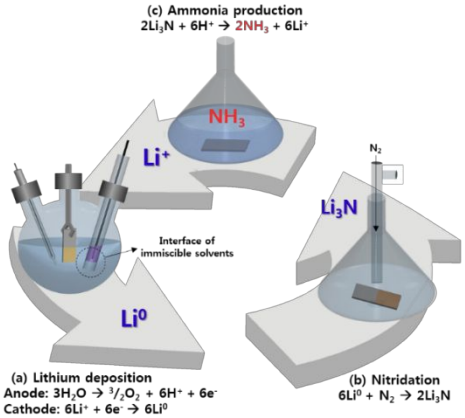

Figure 1. A schematic representation of membrane-free Li-mediated NH_3 synthesis.

As a novel strategy in the Li-mediated ammonia synthesis regime, a membraneless electrochemical cell for Li deposition was proposed which relies on the immiscible nature of aqueous/organic electrolytes. The biphasic interface serves as not only a Li-ion conductor but also a physical barrier, rendering expensive LISICON dispensable and therefore making the membraneless Li-mediated pathway (Figure 1) more economically favorable. Herein, in an effort to realize this membraneless approach, we proved that an aqueous lithium perchlorate ($LiClO_4$) solution and an organic electrolyte, $LiClO_4$ in propylene carbonate (PC), are not miscible but instead form an interface, acting in the same manner as a LISICON-based hybrid aqueous/organic electrolyte system,[25] even without the use of LISICON. $LiClO_4$/PC-based system was chosen as the model electrolyte for its well-understood interfacial chemistry (e.g. the reaction of metallic Li and PC) and already proven applicability toward nitridation and NH_3 synthesis.[25,27] It is worth noting that, by taking advantage of the hydrophobic polymer poly(methyl methacrylate) (PMMA) in the organic phase,[28,29] we successfully controlled the interfacial diffusion of water from the aqueous phase to the organic phase, thereby ensuring the water-proof nature of organic solvent and stability of our biphasic system. Interestingly, the additional benefit of PMMA was that its incorporation to the organic electrolyte enhanced Li plating performance and in turn, NH_3 synthesis efficiency.

Results and discussion

Electrochemical behavior of a biphasic system

Since the density of PC is higher than water (ρ_{PC} = 1.2 g cm^{-3} vs. ρ_{water} = 0.997 g cm^{-3}), the aqueous phase floats on top of the organic electrolyte, thus spontaneously forming a biphasic system without being intermixed (Figure 2(a)). In order to evaluate the general electrochemical behavior of this system, the aqueous/organic electrolytes were individually subjected to cyclic voltammetry (CV) in a three-electrode electrochemical cell (Figure S1) in the potential range of -0.45 to 1.45 V and 3.55 to 5.30 V (vs. Li^+/Li) for the organic and aqueous phase, respectively. As shown in Figure 2(b), the CV of the organic catholyte (red) exhibited a reversible behavior of Li plating and stripping, while the aqueous anolyte (blue) showed current density increase due to oxygen evolution. This result showed that the electrochemical windows for individual electrolytes were separated, demonstrating the immiscible nature of two electrolytes. The position of potentials in the CVs indicated a minimum cell voltage of 4.5 V for Li deposition by utilizing the two immiscible electrolytes system. As shown in Figure S5, the required voltage for Li deposition at 5 mA cm^{-2} was about 5.3 V, which was 14.5% lower than the voltage requirement of LISICON-based Li deposition (6.2 V) at the same current density.[25]

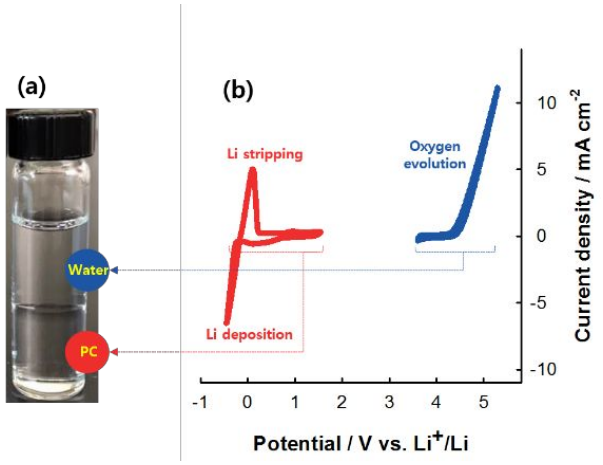

Figure. 2. (a) Immiscibility between water and propylene carbonate; (b) Cyclic voltammetry (CV) of Ni foil in the organic electrolyte (1 M $LiClO_4$/PC + 1wt.% PMMA, red) and Pt wire anode in aqueous electrolyte (1 M $LiClO_4$, blue) performed in the three-electrode electrochemical cell shown in Figure S1 (scan rate: 50 mV s^{-1}).

The effect of PMMA on the stability of a biphasic system

Controlling interfacial water diffusion from aqueous to organic phase is a prerequisite for ensuring the stability of the interface between the two immiscible electrolytes systems. As shown in Figure 3(a), contamination of the organic electrolyte with water caused irreversible loss of metallic Li or electrons, resulting in hydrogen evolution ((i) $H_2O + e^- \rightarrow OH^- + {}^1/_2H_2$ or (ii) $Li^0 + H_2O \rightarrow LiOH + {}^1/_2H_2$) and thus lowering FE. On the other hand, the addition of hydrophobic polymer PMMA rendered the organic electrolyte water-proof and hence protected metallic Li from water-driven attacks (Figure 3(a), right).[28] We firstly demonstrated this based on Li plating efficiencies, measured immediately after establishing the biphasic system and after

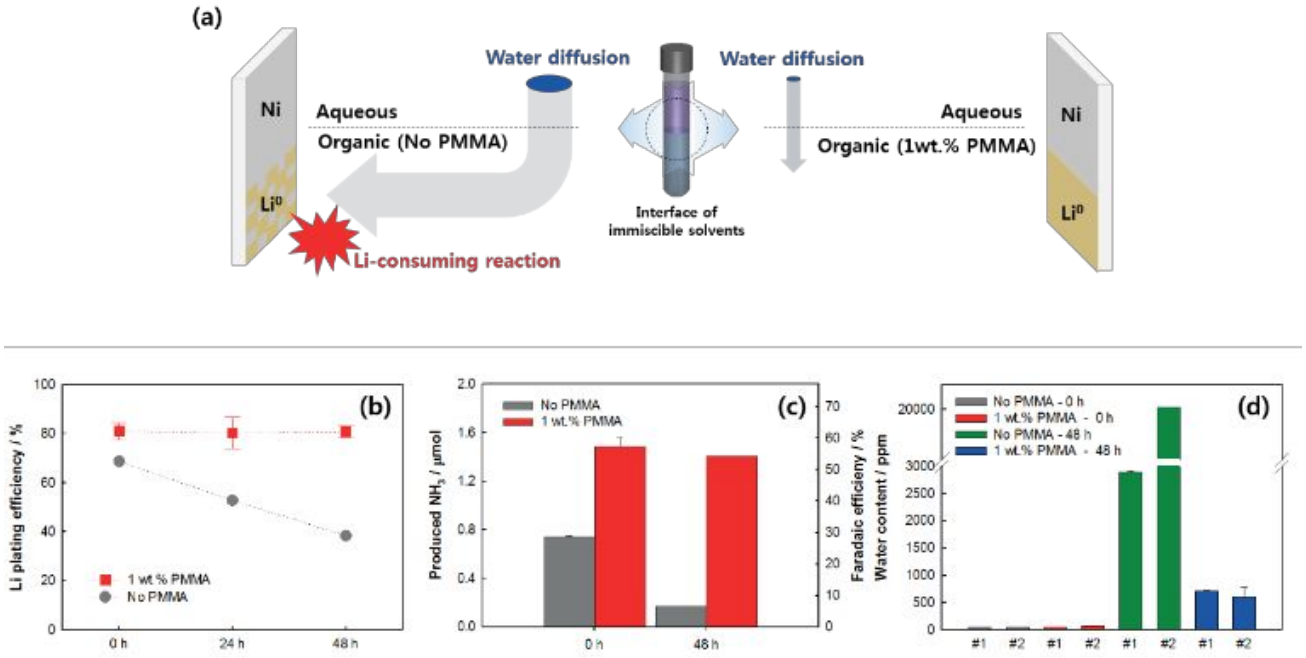

Figure. 3. (a) A schematic illustration showing water diffusion through the interface of the immiscible solvents and the resultant Li-consuming side reaction; (b) Li plating efficiencies of the organic electrolytes (1 M $LiClO_4$/PC) with no and 1 wt.% PMMA after storage times of 0, 24, and 48 hours (see Figure S6(a) and (b) for voltage profiles, capacity: 0.83 mAh cm^{-2}); (c) The amount of NH_3 and corresponding FEs using the organic electrolytes (1 M $LiClO_4$/PC) with no and 1 wt.% PMMA after storage times of 0 and 48 hours (Li capacity: 0.83 mAh cm^{-2}, Li was nitrided at 180 °C for 3 h); (d) Water contamination in the organic electrolytes measured by Karl-Fischer titration (see Table S1 for details).

storage times of 24 and 48 hours (Figure 3(b) and Figure S6(a) and (b)). The initial Li plating efficiencies were 68.7 % and 81.0 % for the organic electrolyte with no and 1 wt.% PMMA, respectively. After a storage time of 48 h, it decreased to 38.4 % without PMMA, while the initial efficiency was retained in the presence of 1 wt.% PMMA, exhibiting 80.8 %. Similar phenomena were also observed in CV analysis (See the caption of Figure S6 (c) and (d)). Note that Li plating efficiency is of great importance since only live metallic Li can be used in the subsequent nitridation and therefore determines the maximum attainable FEs for NH_3 synthesis.[25] As shown in Figure 3(c), the corresponding NH_3 syntheses, obtained after nitridation of Li deposit under N_2 atmosphere, were in accordance with Li plating efficiency: the initial NH_3 syntheses were 7.43×10^{-7} mol and 1.49×10^{-6} mol for organic electrolytes with no PMMA and 1 wt.% PMMA, which correspond to FE of 28.62 % and 57.2 %, respectively. After 48 h, the FE without PMMA diminished to 6.5 %, while the organic medium with 1 wt.% PMMA still showed FE of 54.6 %. All these results demonstrated that the incorporation of PMMA into the organic phase improves the stability of the interface between the two immiscible electrolytes. Karl-Fischer titration analysis supported our hypothesis on PMMA-driven prevention of water contamination (Figure 3(d) and Table S1): at 0 h, the organic phases all exhibited their own dry nature (43.2~71.6 ppm). After 48 h, however, in the absence of PMMA, the organic phase was seriously contaminated with relatively high concentration of water (2912.0~20116.0 ppm), which diffused from the aqueous to organic phase through the interface of the two immiscible electrolytes. Note that the water distribution in the bulky organic phase was inhomogeneous because water transport relied solely on diffusion through the confined interface. On the contrary, the amount of water diffused was far lower (428.0~792.1 ppm) in the presence of 1 wt.% PMMA due to the hydrophobicity of PMMA, which is in accordance with previous report.[28] It is worth emphasizing that slight water contamination (ca. 800 ppm) in PMMA-containing electrolyte had no impact on the performances in terms of Li plating efficiency and NH_3 synthesis (Figure 3(b) and (c)), demonstrating the water-tolerant nature of the PMMA-based electrolyte.[30] Such a water-tolerant feature, as well as the prevention of water contamination with PMMA addition, are undeniable benefits with regard to the survival of metallic Li, especially in our presented membrane-free strategy.

The effect of PMMA on Li plating efficiency and NH_3 production

Interestingly, the presence of PMMA exhibited additional benefit of enhancing Li plating efficiency and NH_3 synthesis; as shown in Figure S7 (and Figure 3(b) and (c)), certain amount of PMMA inclusion (1 wt.%) favored NH_3 synthesis, which diminished at higher PMMA concentrations (2 and 3 wt.%). As can be inferred from the width of semicircles in the electrochemical impedance spectroscopy (Figure S8), which is an indicator of passive film resistance,[31,32] the organic electrolytes with 2 and 3 wt.% PMMA brought about excessive growth of resistive and thick surface layers composed of solid electrolyte interface (SEI) and/or PMMA during Li deposition.[33,34] Excessive growth of such passivation layers is

deemed to hinder the penetration of N_2 into Li layer in the stage of nitridation, thereby leading to poor NH_3 synthesis.

To gain deep insights into how PMMA improved Li plating and NH_3 production, the morphologies of Li deposits with and without 1 wt.% PMMA were visualized using SEM (Figure 4(a) and (b)). The Li deposit without addition of PMMA (Figure 4(a)) exhibited sharp and needle-like dendrites mainly due to the locally enhanced electric field.[35,36] It can be observed that sharp dendrites are prevailing over the entire Ni surface with a deposition capacity of 0.83 mA h cm^{-2} (Figure S9(a)). The dendritic Li deposit with a large surface area can easily trigger the side reactions between metallic Li and the organic electrolyte PC, thereby forming excessive SEI layer which is predominantly composed of Li_2CO_3 and/or $ROCO_2Li$ (R=alkyl) and thus irreversibly decreasing Li plating efficiency and FE for NH_3 synthesis.[37,38] In contrast, the presence of 1 wt.% PMMA obviously brought about much different morphology (Figure 4(b) and Figure S9(b)) though few dendritic structures were still observed: thicker Li particles were partially connected creating an overall flat and smooth layer, contrary to the rough and dendritic morphology in the absence of PMMA. The retarded formation of needle-like dendrites with 1 wt.% PMMA, therefore could reduce the side reactions between Li metal and PC.[37] This was supported by the C1s XPS spectra of the Li deposits (Figure 4(c) and (d)). The carbon peak at 289.9 ± 0.1 eV (red), assigned to Li_2CO_3 and/or $ROCO_2Li$, decreased with the addition of 1 wt.% PMMA, demonstrating that the Li-consuming and carbonates-forming side reactions were largely inhibited in the presence of PMMA.[39]

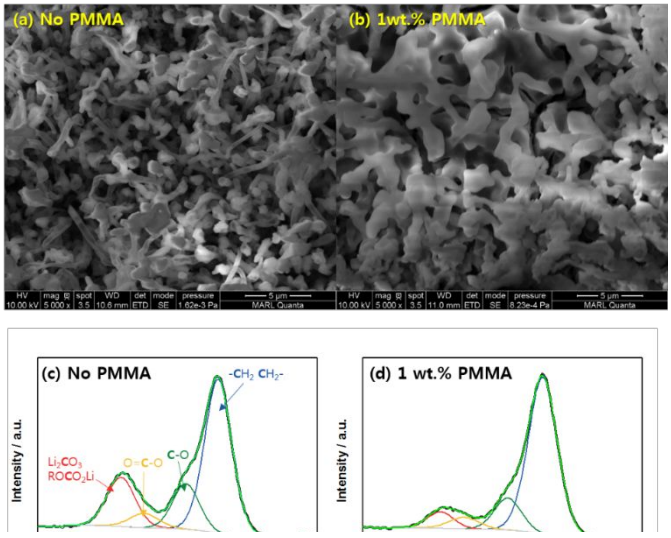

Figure. 4. SEM images of Li deposited (a) in the absence and (b) presence of 1 wt.% PMMA; C1s XPS spectra of Li deposited (c) in the absence and (d) presence of 1 wt.% PMMA (Deposition current density: 5 mA cm^{-2}, Li capacity: 0.83 mAh cm^{-2} for all cases).

The mechanism of PMMA-driven enhancement in Li plating efficiency

PMMA participates in the process of Li deposition and serves as a storage medium for Li-ions as shown in Figure S10.[35,40] In the electrochemical reduction process, PMMA firstly undergoes one-electron transfer reduction and generates intramolecular cyclopentanedione through a ring-closing reaction between two adjacent ester groups, accompanied by irreversible elimination of lithium methoxide (CH_3OLi) (Figure S10(a)).[40] In the next step (Figure S10(b)), reversible lithiation and delithiation processes occur on the as-formed conjugate carbonyl groups through two-electron transfer reactions.[40] Such a Li-ion storage mechanism by PMMA alters the way Li is deposited, which is adequately proven in previous studies with Cu as the substrate.[35] In order to understand the role of PMMA specifically in our experimental conditions, electrochemical behaviors were first investigated using cyclic voltammetry within the voltage window of 0.35 ~ 2.4 V (vs. Li^+/Li) at a scan rate of 10 mV s^{-1} (Figure S11(a)). In the first negative scan, two cathodic peaks were found at 1.40 (peak A) and 0.58 V (peak B), while only one peak at 1.27 V was observed during the first anodic scan. In the second cycle, the sharp cathodic peak A at 1.40 V disappeared, but the cathodic/anodic peaks at 0.58 V and 1.27 V were still observed. Indeed, the sharp cathodic peak A at 1.40 V is ascribed to the formation of intramolecular cyclopentanedione and the elimination of CH_3OLi as shown in Figure S10(a), and its irreversible nature is well reflected on the disappearance of peak A in the second negative sweep.[40] It is worth mentioning that the sharpness of the peak A implies a fast kinetics of this ring-closing reaction.[40] The reduction/oxidation peaks at 0.58 V (peak B) and 1.27 V are due to the reversible lithiation and delithiation that occur on the in-situ formed carbonyl groups via a two-electron transfer reaction, as depicted in Figure S10(b).[40] Likewise, during chronopotentiometry at a current density of 0.05 mA cm^{-2} (Figure S11(b)), two voltage plateaus were found at about 1.35 and 0.63 V before Li deposition, which correspond to the peak A and B from CV analysis, respectively. All these were systematically confirmed and understood via Fourier transform infrared spectroscopy (FT-IR) using Ni electrodes obtained at different stages of charging during the chronopotentiometry experiment. As shown in Figure S11(c), the pristine electrode at open circuit potential exhibited strong vibration bands at 1735 and 1149 cm^{-1}, which can be assigned to C=O stretching of ester carbonyl group and C-O-C vibration, in good accordance with the structure of PMMA.[40] After being charged to 1.0 V (Figure S11(c), red), these two peaks disappeared, and two new peaks appeared at 1650 and 1100 cm^{-1}, which correspond to the keto carbonyl group and C-O vibration from CH_3OLi, respectively.[35,40,41] The occurrence of these new peaks demonstrates the formation of intramolecular cyclopentanedione and CH_3OLi (Figure S10(a)). After being further charged to 0.2 V (Figure S11(c), blue), an additional peak appeared at around 530 cm^{-1}, which indicates that PMMA is lithiated and Li-ion is bound to the carbonyl oxygen.[35] Further characterization using XPS analysis well agreed with the FT-IR results (See the caption of Figure S12). All these characterizations, along with the electrochemical analysis of CV profiles led us to summarize as follows: (1) the formation of intramolecular cyclopentanedione at 1.40 V provides binding sites (carbonyl groups) for Li-ions; (2) Li-ions are bound to PMMA via carbonyl groups and thus immobilized during the reversible lithiation at about 0.58 V; and (3) the Li-ions bound to PMMA are preferentially deposited onto Li particles on the

Ni substrate, providing "active sites" for subsequent deposition and serving to escort the way of next Li-ions to be deposited.[35] Considering that those "active sites" are distributed throughout the three-dimensional molecular structure of PMMA, the final morphology of Li deposit is patterned after the PMMA structure[35], and this could explain the morphology of interconnected Li particles with a smooth surface (Figure 4(b)), which is contrary to the needle-like individual dendrites due to enhanced electric field in the absence of PMMA (Figure 4(a)).

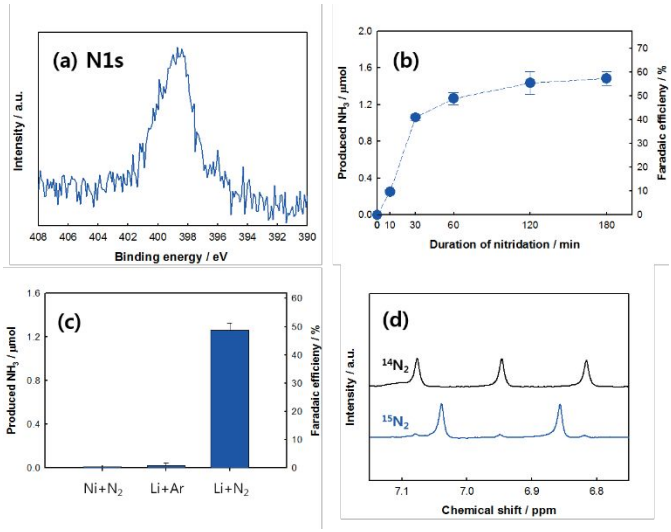

Figure. 5. (a) N1s XPS spectra of the Li deposit nitrided at 180 °C; (b) the amounts of synthesized NH_3 and corresponding FEs using Li deposit nitrided at 180 °C over time; (c) the amount of synthesized NH_3 and corresponding FEs using Ni or Ar as a reactant in control experiments; (d) ^1H NMR spectra of the sulfuric acid solutions after the hydrolysis of Li_3N, which were generated during nitridation using $^{14}N_2$ and $^{15}N_2$. (Li was deposited from 1 M $LiClO_4$/PC + 1 wt.% PMMA and Li capacity was 0.83 mAh cm^{-2} for all cases).

NH_3 synthesis performance and control experiments

During nitridation, higher amount of NH_3 synthesis was obtained with increased nitridation temperature (Figure S13), which is in accordance with previous literatures.[24,25] As supported by the N1s XPS spectrum (Figure 5(a)), Li_3N was truly the intermediate of Li-mediated NH_3 synthesis (398.3 eV).[42] Figure 5(b) illustrates NH_3 synthesis and corresponding FEs when Li deposit was nitrided at 180 °C for different time periods. The rate of NH_3 production decreased over time, as a consequence of decreasing accessibility of N_2 to active Li metal, due to the hindrance by SEI layer as well as newly formed Li_3N layer.[25] The maximum attainable FE after 3 h nitridation was 57.2 % (Figure 5(b)). We believe that the loss in FE is ascribed to: (1) Li-consuming and carbonate-generating SEI formation, as reflected in the Li plating efficiency (Figure 3(b)); and (2) exposure of Li to the air especially during the transfer of Li from the electrochemical cell to the nitridation chamber. NH_3 synthesis rate was calculated based on a nitridation time of 1 h (see section 1.5. of the Supplementary Information); it turned out to be 1.21×10^{-9} mol s^{-1} cm^{-2}, but this can be further enhanced provided that the three sub-processes were operated simultaneously at higher current density for Li deposition.

In this study, particular attention was paid to systematically prove that N_2 is the dominant nitrogen source for NH_3 synthesis[43-45]; we carried out several rigorous control and confirmatory experiments specifically in the stage of nitridation. As shown in Figure 5(c), the replacement of Li deposit with pristine Ni or replacement of N_2 flow with argon resulted in negligible NH_3 synthesis; only the exposure of N_2 to metallic Li led to NH_3 synthesis, confirming that the formation of Li_3N is unquestionably attributed to the bulk reaction between metallic Li and N_2. Most conclusively, as shown in the ^1H NMR spectra (Figure 5(d)), the hydrolyzed Li_3N, prepared under the nitridation of Li using $^{15}N_2$, showed a doublet corresponding to ^{15}N-^1H coupling, while only a triplet corresponding to ^{14}N-^1H coupling was observed using $^{14}N_2$, qualitatively verifying that NH_3 is originated from N_2.[26] Furthermore, isotope-labelled quantification well agreed with the colorimetric NH_3 assay using the indophenol blue method (Figure S14). All these stringent control experiments prove the NH_3 synthesis is truly via a so-called Li-mediated pathway ($Li^+ \rightarrow Li \rightarrow Li_3N \rightarrow NH_3$).

For the last few years, extensive efforts have been made for the improvement of electrochemical nitrogen reduction, with the majority focusing on the development of novel electrocatalysts. The catalyst synthesis processes are usually complicated and rely on the use of toxic or hazardous compounds (i.e. pyromellitic dianhydride[14], cetyltrimethylammonium bromide[15], N, N-dimethylformamide[16], and ethylene glycol[17,22]). Our Li-mediated process does not need costly nanoparticle synthesis process, but just employs a green solvent PC[46], whose production could even utilize carbon dioxide.[47] While the durability of electro-catalysts are questionable, PC can be reused, and in particular, Li salt could be efficiently recycled in the Li-mediated approach as demonstrated in XRD[24] and ICP[25] analysis. With its fairly high or comparable performance in terms of synthesis rate and FE compared to the state-of-the-art technologies (Table S2), this study proves the advantageous features as one of the most advanced and reliable electrochemical process for N_2 fixation. Although the estimated energy consumption required for Li deposition is slightly larger than that of matured Haber-Bosch process[24,25,48] Li-mediated NH_3 electrosynthesis route offers significant benefits compared to the traditional thermochemical process, such as no carbon emission (if powered by renewable wind and solar electricity, and indeed, carbon dioxide is utilized for the production of PC), no need for fossil sources as hydrogen source, milder operating conditions, and possibility of storing renewable energy, thereby enabling small scale, distributed, decentralized, onsite production of NH_3, with reduced transportation and distribution costs.[24,25]

Conclusion

In summary, we proposed a membrane-free approach for ambient Li deposition based on the immiscibility of aqueous/organic electrolytes and demonstrated the applicability of the biphasic system for the realization of Li-mediated ammonia synthesis. The behavior of this system is the same as a LISICON-based cell,[25] especially thanks to the stability

of the biphasic system. Rather, this system requires lower cell voltage (5.3 V in this study vs. 6.2 V in LISICON-based cell at 5 mA cm^{-2}), even without the need of expensive membrane, rendering it more economically favorable. The FE and NH_3 synthesis rate (57.2 % and 1.21 × 10^{-9} mol $cm^{-2}s^{-1}$, respectively) obtained using a proof-of-concept electrochemical cell are higher or comparable with many of recent reports on NH_3 synthesis. This proof-of-concept has been realized merely using our model hybrid electrolytes system ($LiClO_4$ and PC-H_2O), but the use of the best optimized electrolytes with better biphasic stability, higher conductivity, higher stability against Li (lower SEI formation), and applicability to a continuous, integrated process will achieve further improvements in the novel Li-mediated NH_3 synthesis.

Conflicts of interest

The authors claim no conflicts of interest.

Acknowledgements

This research was partly funded by the ARPA-E REFUEL program (under the contract of DE-AR0000818). W. Li acknowledges Iowa Economy Development Authority (IEDA) for its cost share fund, and his Richard Seagrave Professorship fund. We thank Dr. Feng Zhao and Jared Liao from Storagenergy Technologies, Inc for their fruitful discussion on ammonia electrosynthesis and quantification; and we are grateful to Prof. Jared L. Anderson and Mr. Muhammad Q. Farooq for their Karl-Fischer titration analysis, and Dr. Dapeng Jing for XPS characterizations in this publication. K. Kim acknowledges Rebecca Kim for her devotion to artworks.

Notes and references

1 Food and Agriculture Organization of United Nations. (2017). World fertilizer trends and outlook to 2020. http://www.fao.org/3/ai6895e.pdf
2 S. Licht, B. Cui, B. Wang, F.-F. Li, J. Lau and S. Liu, *Science*, 2014, **345**, 637–640.
3 V. Kyriakou, I. Garagounis, E. Vasileiou, A. Vourros and M. Stoukides, *Catalysis Today*, 2017, **286**, 2–13.
4 I. J. McPherson, T. Sudmeier, J. Fellowes and S. C. E. Tsang, *Dalton Transactions*, 2019, **48**, 1562–1568.
5 J. G. Chen, R. M. Crooks, L. C. Seefeldt, K. L. Bren, R. M. Bullock, M. Y. Darensbourg, P. L. Holland, B. Hoffman, M. J. Janik, A. K. Jones, M. G. Kanatzidis, P. King, K. M. Lancaster, S. V. Lymar, P. Pfromm, W. F. Schneider, R. R. Schrock, *Science,* 2018, **360**, 873.
6 J. Deng, J. A. Iñiguez and C. Liu, *Joule*, 2018, **2**, 846–856.
7 S. Giddey, S. P. S. Badwal and A. Kulkarni, *International Journal of Hydrogen Energy*, 2013, **38**, 14576–14594.
8 K. Kugler, B. Ohs, M. Scholz and M. Wessling, *Phys. Chem. Chem. Phys.*, 2014, **16**, 6129–6138.
9 K. Kim, J.-N. Kim, H. C. Yoon and J.-I. Han, *International Journal of Hydrogen Energy*, 2015, **40**, 5578–5582
10 A. Züttel, A. Remhof, A. Borgschulte and O. Friedrichs, *Philosophical Transactions of the Royal Society A: Mathematical, Physical and Engineering Sciences*, 2010, **368**, 3329–3342.
11 M. A. Shipman, M.D. Symes, *Catalysis Today*, 2017, **286**, 57-68.
12 K. Kim, C.-Y. Yoo, J.-N. Kim, H. C. Yoon and J.-I. Han, *Korean Journal of Chemical Engineering*, 2016, **33**, 1777–1780.
13 S. Chen, S. Perathoner, C. Ampelli, C. Mebrahtu, D. Su and G. Centi, *Angewandte Chemie International Edition*, 2017, **56**, 2699–2703.
14 G.-F. Chen, X. Cao, S. Wu, X. Zeng, L.-X. Ding, M. Zhu and H. Wang, *Journal of the American Chemical Society*, 2017, **139**, 9771–9774.
15 D. Bao, Q. Zhang, F.-L. Meng, H.-X. Zhong, M.-M. Shi, Y. Zhang, J.-M. Yan, Q. Jiang and X.-B. Zhang, *Advanced Materials*, 2017, **29**, 1604799.
16 C. Lv, C. Yan, G. Chen, Y. Ding, J. Sun, Y. Zhou and G. Yu, *Angewandte Chemie International Edition*, 2018, **57**, 6073–6076.
17 J. Wang, L. Yu, L. Hu, G. Chen, H. Xin and X. Feng, *Nature Communications*, 2018, **9**, 1795.
18 F. Zhou, L. M. Azofra, M. Ali, M. Kar, A. N. Simonov, C. McDonnell-Worth, C. Sun, X. Zhang and D. R. MacFarlane, Energy & Environ. Sci., 2017, **10**, 2516-2520
19 K. Kim, N. Lee, C.-Y. Yoo, J.-N. Kim, H. C. Yoon and J.-I. Han, *Journal of The Electrochemical Society*, 2016, **163**, F610–F612.
20 X. Yang, J. Nash, J. Anibal, M. Dunwell, S. Kattel, E. Stavitski, K. Attenkofer, J. G. Chen, Y. Yan and B. Xu, *Journal of the American Chemical Society*, 2018, **140**, 13387–13391.
21 K. Kim, C.-Y. Yoo, J.-N. Kim, H. C. Yoon and J.-I. Han, *Journal of The Electrochemical Society*, 2016, **163**, F1523–F1526.
22 Y.-C. Hao, Y. Guo, L.-W. Chen, M. Shu, X.-Y. Wang, T.-A. Bu, W.-Y. Gao, N. Zhang, X. Su, X. Feng, J.-W. Zhou, B. Wang, C.-W. Hu, A.-X. Yin, R. Si, Y.-W. Zhang and C.-H. Yan, *Nature Catalysis*, DOI:10.1038/s41929-019-0241-7.
23 B. Cui, J. Zhang, S. Liu, X. Liu, W. Xiang, L. Liu, H. Xin, M. J. Lefler and S. Licht, *Green Chemistry*, 2017, **19**, 298–304.
24 J. M. McEnaney, A. R. Singh, J. A. Schwalbe, J. Kibsgaard, J. C. Lin, M. Cargnello, T. F. Jaramillo and J. K. Nørskov, *Energy & Environmental Science*, 2017, **10**, 1621–1630.
25 K. Kim, S. J. Lee, D.-Y. Kim, C.-Y. Yoo, J. W. Choi, J.-N. Kim, Y. Woo, H. C. Yoon and J.-I. Han, *ChemSusChem*, 2018, **11**, 120–124.
26 N. Lazouski, Z. J. Schiffer, K. Williams and K. Manthiram, *Joule*, 2019, **3**, 1127–1139.
27 K. Kim, H. Cho, S. H. Jeon, S. J. Lee, C.-Y. Yoo, J.-N. Kim, J. W. Choi, H. C. Yoon and J.-I. Han, *Journal of The Electrochemical Society*, 2018, **165**, F1027–F1031.
28 B. Wu, X. Chen, C. Zhang, D. Mu and F. Wu, *New Journal of Chemistry*, 2012, **36**, 2140.
29 S. M. Simon, A. Chandran, G. George, M. S. Sajna, P. Valparambil, E. Kumi-Barmiah, G. Jose, P. R. Biju, C. Joseph and N. V. Unnikrishnan, *ACS Omega*, 2018, **3**, 14924–14932.
30 R. Kerr, N. Singh, T. S. Arthur, T. Pathirana, F. Mizuno, K. Takechi, M. Forsyth and P. C. Howlett, *Sustainable Energy & Fuels*, 2018, **2**, 2276–2283.
31 Q. Lu, J. Yang, W. Lu, J. Wang and Y. Nuli, *Electrochimica Acta*, 2015, **152**, 489–495.
32 D. Lin, J. Zhao, J. Sun, H. Yao, Y. Liu, K. Yan and Y. Cui, *Proceedings of the National Academy of Sciences*, 2017, **114**, 4613–4618.
33 C. Tang, Y. Ren, Z. Chen and J. Ding, *Ionics*, 2019, **25**, 1007–1014.
34 B. H. Shen, G. M. Veith and W. E. Tenhaeff, *Scientific Reports*, 2018, **8**, 11549.
35 Y. Guo, Y. Ouyang, D. Li, Y. Wei, T. Zhai and H. Li, *Energy Storage Materials*, 2019, **16**, 203–211.
36 F. Ding, W. Xu, G. L. Graff, J. Zhang, M. L. Sushko, X. Chen, Y. Shao, M. H. Engelhard, Z. Nie, J. Xiao, X. Liu, P. V. Sushko, J.

Liu and J.-G. Zhang, *Journal of the American Chemical Society*, 2013, **135**, 4450–4456.
37 R. Zhang, N.-W. Li, X.-B. Cheng, Y.-X. Yin, Q. Zhang and Y.-G. Guo, *Advanced Science*, 2017, **4**, 1600445.
38 J. Qian, W. A. Henderson, W. Xu, P. Bhattacharya, M. Engelhard, O. Borodin and J.-G. Zhang, *Nature Communications*, 2015, **6**, 6362.
39 F. Liao, J. Światowska, V. Maurice, A. Seyeux, L. H. Klein, S. Zanna and P. Marcus, *Electrochimica Acta*, 2014, **120**, 359–368.
40 Y. Wang, L. Zhang, L. Zhang, F. Zhang, P. He, H. Zheng and H. Zhou, *Advanced Energy Materials*, 2016, **6**, 1601375.
41 V. Boiadjiev and W. T. Tysoe, *Chemistry of Materials*, 1998, **10**, 334–344.
42 L. Wang, J. Liu, S. Yuan, Y. Wang and Y. Xia, *Energy & Environmental Science*, 2016, **9**, 224–231.
43 B. H. R. Suryanto, H.-L. Du, D. Wang, J. Chen, A. N. Simonov and D. R. MacFarlane, *Nature Catalysis*, 2019, **2**, 290–296.
44 L. F. Greenlee, J. N. Renner and S. L. Foster, *ACS Catalysis*, 2018, **8**, 7820–7827.
45 S. Z. Andersen, V. Čolić, S. Yang, J. A. Schwalbe, A. C. Nielander, J. M. McEnaney, K. Enemark-Rasmussen, J. G. Baker, A. R. Singh, B. A. Rohr, M. J. Statt, S. J. Blair, S. Mezzavilla, J. Kibsgaard, P. C. K. Vesborg, M. Cargnello, S. F. Bent, T. F. Jaramillo, I. E. L. Stephens, J. K. Nørskov and I. Chorkendorff, *Nature*, DOI:10.1038/s41586-019-1260-x.
46 H. L. Parker, J. Sherwood, A. J. Hunt and J. H. Clark, *ACS Sustainable Chem. Eng.*, 2014, **2**, 1739–1742.
47 L. Guo, L. Deng, X. Jin, Y. Wang and H. Wang, *RSC Adv.*, 2018, **8**, 26554–26562.
48 G. Soloveichik, *Nat Catal*, 2019, **2**, 377–380.